ISSN 0915-633X

NATIONAL INSTITUTE FOR FUSION SCIENCE

Molecular Dynamics and Structure Organization in Strongly-Coupled Chain of Charged Particles

M. Tanaka, A.Yu Grosberg, V.S. Pande and T. Tanaka

(Received - June 18, 1997)

NIFS-498 July 1997

RESEARCH REPORT
NIFS Series

NAGOYA, JAPAN

Molecular Dynamics and Structure Organization in Strongly-Coupled Chain of Charged Particles

Motohiko Tanaka, A.Yu Grosberg[1], V.S.Pande[2] and Toyoichi Tanaka[1]

National Institute for Fusion Science, Toki 509-52, Japan

[1]Massachusetts Institute of Technology, Cambridge, MA 02139, USA

[2]University of California at Berkeley, Berkeley, CA 94720, USA

Abstract

The dynamical and equilibrium properties of a strongly-coupled chain of charged particles (polyampholyte) submerged in a viscous medium are studied using the molecular dynamics simulations. The polyampholyte relaxes to an equilibrium conformation typically in $300\omega_{pe}^{-1}$ due to folding of the chain for low temperatures, and expands several times faster for high temperatures, where ω_{pe} is the plasma frequency. Three regimes with distinct conformations as stretched, oblate and spherical are observed under the Coulomb force at high, medium and low temperatures, respectively. The change in the conformations is considered to minimize the free energy through the electrostatic potential. The gyration radius in these regimes is scaled, respectively, as $R_g \sim N^{1/2}$, $(NT)^{1/3}$, and $N^{0.3}T^{0.8-1.0}$, where N is the number of monomers on the chain and T the temperature. The regime boundaries are characterized by the unique values of the monomer distance $2R_g/N^{1/3}$, being insensitive to the length and stiffness of the chain. The present molecular dynamics agrees well with the Flory theory in the high and medium temperature regimes. The densely-packed frozen state at low temperatures is first obtained here without the use of the lattice model. The transition among the different regimes under the Coulomb force is exactly reversible. However, the transition under the cooperation of the Coulomb force and the attractive short-range force exhibits a hysteresis against successive changes in temperature.

Keywords: Coulomb System, Structure Organization, Phase Transition.

1. Introduction

The strongly-coupled Coulomb plasmas are found in condensed matters, highly compressed laser-irradiated plasmas and the stellar interiors[1-3]. In these circumstances, the Coulomb interactions organize the structure of matters and determine their equilibrium properties. The polyampholyte to be studied in this paper is a chain of electrically charged monomers that represent one or group of atoms or molecules. The monomers connected by the molecular binding force are either positively or negatively charged to have little net charges on the chain[4]. The polyampholyte is an idealization of material polymers[5,6], proteins and nucleic acids like DNAs in biochemical systems[7]. Such polyampholytes are usually submerged in a viscous medium (solvent) which works as thermal reservoir to exert random thermal forces and frictions on them[8].

The most basic issues of the polyampholytes are the formation of equilibrium conformations and dynamical paths toward such states under the long-range Coulomb force and other short-range forces. Further questions are the dependence of the final equilibrium states on the initial conformations and randomness of the charge sequences, and reversibility of the transition among the equilibrium states that is invoked by temperature changes. The last issue relates to an existence of the meta-stable states or the local energy minima. This paper will attempt to answer these questions.

For the polyampholytes, the number of charged monomers in the Debye sphere is typically of the order of unity. The polyampholyte chain is not considered as continuous medium, in sharp contrast with ordinary high-temperature plasmas[9]. For this reason, the direct Coulomb interactions between the charged monomers play the major roles in the structure organization, which need to be calculated with high accuracy in numerical computations. The dynamics of the polyampholyte chain with finite size monomers is governed by the electrostatic and thermal interactions, which is characterized by the coupling constant $\Gamma = e^2/aT$ and the stiffness of the chain v/a^3. Here, e is electron charge, a the monomer distance, v the volume of the monomer, and T the temperature.

The molecular dynamics (particle simulation), which is a tool adopted in this study,

integrates the Newton's equations of motion in time to trace the dynamical evolution of the N-body system. With the method, we are able to study dynamical and equilibrium properties, reaction and relaxation processes along the dynamical paths. Traditionally, the Monte Carlo simulation with the lattice model has widely been used, where a static path search is made among randomly generated new positions of the monomers by following the energy principle; the system should evolve toward the lower energy state. Although the Monte Carlo simulation with the lattice model was useful in predicting the properties of flexible polymers with $v/a^3 \leq 1$, it did not include dynamical effects and may eliminate densely-packed states of stiff polymers at low temperatures.

The outline of this paper will be the following. In Sec.2, the equations used in the present molecular dynamics simulations are presented. We include (1) the long-range electrostatic (Coulomb) force, (2) the harmonic binding force between the adjacent monomers, and (3) the random thermal kicks and the frictional force originating from the surrounding medium. In Sec.3, we will examine the dynamics and equilibrium of a chain of charged N-body system. The relaxation to equilibrium conformations occurs in $200 \sim 300\omega_{pe}^{-1}$ due to folding of the chain, and the expansion at high temperatures is several times faster, where ω_{pe} is the plasma frequency. Three temperature regimes of the polyampholytes with different conformations and parameter dependences are observed. The free energy is minimized through the electrostatic potential by the change in the conformations. Good agreements between the molecular dynamics simulation and the Flory theory of the polyampholyte[10] are confirmed in the high and medium temperature regimes. On the other hand, the densely-packed "frozen" state at low temperatures is found for the first time in the present study that does not adopt the lattice model (Sec.3(b)). Then, in Sec.4 we will add the short-range attractive force to find the cooperative effects of the long and short-range forces. A hysteresis of the transition path among the equilibrium states is demonstrated. Sec.5 will be a conclusion of this paper.

2. The System Equations

For the purpose of studying the dynamical evolution and equilibrium properties of the polyampholytes[11], we solve the equations of motion for the positions and velocities of the N monomers. The equations for the i-th monomer ($i = 1, ..., N$) is written,

$$m\frac{d\mathbf{v}_i}{dt} = \mathbf{F}_{LR}(\mathbf{r}_i) - \frac{3T}{a^2}(2\mathbf{r}_i - \mathbf{r}_{i+1} - \mathbf{r}_{i-1}) + \mathbf{F}_{th} - \nu m\mathbf{v}_i, \tag{1}$$

$$\frac{d\mathbf{r}_i}{dt} = \mathbf{v}_i. \tag{2}$$

The electrostatic Coulomb force, which is a long-range force, is given by

$$\mathbf{F}_{LR}(\mathbf{r}_i) = \sum_j \frac{Z_i Z_j e^2}{|\mathbf{r}_i - \mathbf{r}_j|^2}\hat{\mathbf{r}_{ij}}. \tag{3}$$

Here, $\mathbf{r}_i$ and $\mathbf{v}_i$ are the position and velocity of the i-th monomer, respectively, m, Z_i are mass and charge state ($Z_i = \pm 1$ is assumed), $\hat{\mathbf{r}}_{ij}$ is a unit vector along $(\mathbf{r}_i - \mathbf{r}_j)$, and ν is the friction constant. In Eq.(3), the Coulomb force is summed over all the possible monomer pairs, and the harmonic spring force connecting the monomers is calculated pairwise. The thermal force $\mathbf{F}_{th}$ that acts on the monomers is generated using random numbers and constitutes a Gaussian distribution in each time step. The thermal and friction forces exerted by the surrounding medium serve as the reservoir to maintain the momentum and kinetic energy of the N-body system at the thermal equilibrium level.

It is emphasized that the monomers on the chain can occupy any point in the six-dimensional space $(\mathbf{r}, \mathbf{v})$, unlike the lattice model[5] which restricts the direction, distance and number of the close neighbors, especially in the dense state. The minimum distance allowed for any pair of the monomers is $a_{col} = 0.2a$ or $0.5a$, below which the monomers are elastically scattered. The stiffness of the chain in our simulation then becomes $v/a^3 = (\pi/6)(a_{col}/a)^3 \sim 0.004 - 0.065$, which well represents those values obtained by laboratory experiments, i.e., $v/a^3 \leq 0.2$ for most flexible monomers, and $v/a^3 \sim 0.003$ for double helix DNA[8].

All the simulation quantities in Sec.3 and 4 are normalized as non-dimensional ones (the $(\hat{})$ quantities):

$$\mathbf{r} = a\hat{\mathbf{r}},\ \mathbf{v} = a\omega_p\hat{\mathbf{v}},\ t = \hat{t}\omega_p^{-1}, \tag{4}$$

with $\omega_p = \sqrt{4\pi n_0 e^2/m}$ being the plasma frequency and n_0 the initial particle number density. Under this normalization, the equations of motion are written (the symbol ($\hat{}$) is suppressed hereafter),

$$\frac{d\mathbf{v}_i}{dt} = \mathbf{F}_{LR}(\mathbf{r}_i) - \frac{3}{4\pi\Gamma}(2\mathbf{r}_i - \mathbf{r}_{i+1} - \mathbf{r}_{i-1}) + \mathbf{F}_{th} - \xi\mathbf{v}_i, \tag{5}$$

$$\frac{d\mathbf{r}_i}{dt} = \mathbf{v}_i, \qquad \mathbf{F}_{LR}(\mathbf{r}_i) = \frac{1}{4\pi}\sum_j \frac{Z_i Z_j}{|\mathbf{r}_i - \mathbf{r}_j|^2}\hat{\mathbf{r}_{ij}}. \tag{6}$$

We see in Eq.(5) that there are two controlling parameters,

$$\Gamma = \frac{e^2}{aT}, \qquad \xi = \frac{\nu}{\omega_p}. \tag{7}$$

Γ is the so-called coupling constant which is an inverse of temperature T. In high-temperature plasmas, the condition $\Gamma \ll 1$ is always satisfied to ensure shielding of the electric field beyond the Debye length[9]. However, the Debye shielding is incomplete in the polymer system as the Debye sphere contains only few monomers.

3. Dynamical and Equilibrium Properties due to the Coulomb Force

(a) Dependence on the Charge Imbalance

The temporal evolution of the polyampholyte chains and their equilibrium properties under the long-range Coulomb force are examined at fixed temperature. The temperature for the run depicted in Fig.1 is $T = \frac{1}{2}T_0$ (the coupling constant $\Gamma = e^2/aT = 2$), the exclusion length is $a_{col} = 0.2a$, and the friction constant is $\xi = 1.0$, where the base temperature T_0 corresponds to $\Gamma_0 = e^2/aT_0 = 1$. The net charge of this chain consisting of randomly distributed 256 charged monomers is 1.6%. In Fig. 1 and the following figures, the (+) and the dot on the chain represent the positive and negative monomers, respectively. For the chosen parameters, the initial conformation in Fig.1(a) is organized to form a spherical and compact globule in fairly a short time which, however, is much longer than the frictional time ξ^{-1}. The conformation at $\omega_{pe}t = 50$ shown in Fig.1(b) is already close to the final and equilibrium conformation of Fig.1 (c).

The time histories of the kinetic energy, the elastic (spring) energy, the electrostatic potential, and the gyration radius defined by $R_g = (\sum_i(\mathbf{r}_i - < \mathbf{r} >)^2)^{1/2}$ are depicted

in Fig.2 for the above polyampholyte. The average kinetic energy per monomer is held constant, $W_{kin} \sim \frac{3}{2}T$, by the thermal kicks and the frictional force, as seen in Fig.2(a). The elastic energy which is proportional to the square of the average distance between the connected monomers increases quickly in the initial transient phase of $t < 20\omega_{pe}^{-1}$, and is fixed almost at a constant level such that energy equi-partition is maintained during the run, $W_{kin} \sim W_{spr}$. Also, the electrostatic potential and the radius relax to equilibrium values, whose relaxation (e-folding) time $\tau_{rel} \sim 280\omega_{pe}^{-1}$ is long compared to that of the elastic energy. Oscillating fluctuations with $\tau_{N=256} = 130 \sim 170\omega_{pe}^{-1}$ are observed for $N = 256$ in Fig.2(c) and (d), whereas the oscillation period for $N = 64$ is $\tau_{N=64} \sim 80\omega_{pe}^{-1}$. The oscillation period is proportional to $\sqrt{N}$, implying that the mass (length) of the oscillating sub-chains is proportional to the total mass (length) of the chain N.

The observed two relaxation mechanisms in the short and long time-scales, respectively, are the local adjustment of the connected monomer distances by elasticity, and the global structure organization due to folding of the chain under the Coulomb force.

Figure 3 shows the equilibrium conformations and the time histories of the corresponding gyration radius of the 256-mer chains for the net charge (a) $\delta N/N$ =1.6%, (b) 6.3%, and (c) 14.1%. (The scale of the three-dimensional plot (c) is reduced to about half the original size.) The gyration radius decreases to $R_g \sim 2.3a$ for (a), but increases to $R_g \sim 13a$ for (c). The equilibrium conformation is a spherical and compact globule for the chain with a small charge imbalance of Fig.3(a). For this case, the restoring force by the elasticity which is provided by the harmonic springs overcomes the electrostatic repulsive force. The gyration radius for the case with intermediate charge imbalance in Fig.3(b) undergoes amplitude oscillations whose period is $200\omega_{pe}^{-1}$. When the charge imbalance is larger, the gyration radius increases monotonically as shown in Fig.3(c) and the chain becomes highly stretched. The relaxation time of the structure for these 256-mers is $\tau_{rel} = 200 \sim 300\omega_{pe}^{-1}$. The criterion for the collapse and expansion against the charge imbalance agrees with the Monte Carlo simulation[5]. A simple theory based on the energy principle and valid for the non-neutral polyampholyte predicts that the bifurcation of the compact and stretched configurations occurs at the charge imbalance of $\delta N \sim \sqrt{N}$. If the number of the excess

charge is assumed to be N^{α}, the free energy is given by the sum of the electrostatic and elastic terms,

$$F = e^2 N^{2\alpha}/R + (3T/2)NR^2/a^2. \tag{8}$$

By differentiating the free energy in terms of the average monomer distance R and equating it with zero, one obtains $R \sim (e^2a^2/3T)^{1/3}N^{(2\alpha-1)/3}$. In order for the polyampholyte not to collapse or expand, one must have $\alpha = \frac{1}{2}$. The critical radius is, $R_c \sim (e^2a^2/3T)^{1/3} = a(\Gamma/3)^{1/3}$. In the present simulation, the excess charge of $\delta N = N^{1/2}$ corresponds to $\delta N/N$ =6.3% at which the bifurcation of the equilibrium conformations did occur, as in Fig.3(b).

For the runs shown above, the connected-monomer distances are nearly constant at $d \sim 1.6a$ during the time evolution, while the polyampholytes either shrink or expand depending on the amount of their charge imbalance. Thus, the large change in the structure is due to folding or unfolding of the chain. For the case with a small net charge, it is possible for the charged monomers to find their optimal positions so that one charged monomer is nested among those with the opposite charge sign to minimize the electrostatic energy. Loose aggregates of the positively and negatively charged monomers are created.

The effects of the electrostatic force on the equilibrium properties are further studied in a statistical fashion. A set of the 300 non-neutral polyampholytes of 64-mers having random conformations and charge sequences is generated as the initial condition of molecular dynamics simulations. The temperature of the system is $T = (1/5)T_0$ (corresponding to $\Gamma = 5$) and the exclusion length is $a_{col} = 0.5a$.

Figure 4(a) depicts the case distribution of the polyampholyte chains against their net charge, which is essentially a Gaussian distribution centered at $\delta N = 0$. The critical charge imbalance for the 64-mers is calculated to be $\delta N_c/N$ ~13%. The gyration radius R_g at equilibrium in Fig.4(b) is smallest when the polyampholyte is charge neutral. When the charge imbalance exceeds the critical value, the size of the polyampholyte increases drastically. For example, the gyration radius at $\delta N/N \sim 0.31$ is 3.8 times that of the neutral case. The connected monomer distance $< \Delta r >$ in Fig.4(c) becomes only 1.1 times.

Similarly, the volume $< V >$ that is a sum of the small cubes $(2a)^3$ occupied by at least one monomer of the chain becomes 1.7 times that of the neutral case. The observed relation $R_g^3 \gg <V>$ shows that large increase in the size with temperature is due to unfolding of the chain, instead of isotropic swelling, as shown previously[5]. (The gyration radius is related to the volume by $<V> \sim R_g^3$ if the polyampholyte is spherical, but it tends to give the largest distance between the monomers if the chain is highly stretched.)

The average electrostatic potential depicted in Fig.4(d) is defined by,

$$\Phi = \sum_{ij} Z_i Z_j e^2 / |\mathbf{r}_i - \mathbf{r}_j|. \tag{9}$$

The potential measured from the bottom (charge neutral case) increases with the amount of charge imbalance, $\Delta\Phi \sim 5.0 \times 10^{-2}$ as $\delta N/N = 0 \to 0.31$. The elastic energy, $W_{spr} = (3T/2a^2) < (\Delta r)^2 >$, increases by $\Delta W_{spr} \sim 1.4 \times 10^{-2}$ which is a quarter of the increase in the electrostatic potential. Thus, the electrostatic force is greatly contributing to organize the structure of the polyampholytes when the temperature is low, $T \leq T_0$, or $\Gamma > 1$.

We note in passing that the sign of the potential Φ is negative as a whole. However, if we limit the summation over the monomer pairs with $|\mathbf{r}_i - \mathbf{r}_j| \geq 2R_g/N^{1/3}$, the sign of the potential turns to be positive (repulsive) for $\delta N \gg 1$. This procedure excludes large contribution of the aggregated monomer pairs to the electrostatic potential. This large-scale potential Φ_L actually organizes the global structure of the polyampholytes.

When the temperature is high, the magnitude of the changes in the gyration radius, the monomer distance and the electrostatic potential is small compared to those shown in Fig.4. But, the overall tendency stays qualitatively the same. Also, we remark that the equilibrium properties of the polyampholyte presented in Sec.3 do not depend on the initial conformations. Although each final conformation is affected by the charge sequence, the deviation is eliminated by ensemble average over the randomly generated sequences which constitute the Gaussian distribution in thermal equilibrium.

(b) Temperature Dependence

Now we trace the dynamical evolution of the polyampholytes by the molecular dynamics

and retrieve their equilibrium properties under various temperatures. Figure 5 depicts the typical equilibrium conformations and corresponding velocity distribution functions of the neutral 256-mers with $a_{col} = 0.5a$ in the high and low temperature regimes. For $T/T_0 = 2$ shown in Fig.5(a), the equilibrium conformation is quite stretched. The time evolution of the gyration radius for the high-temperature regime varies substantially depending on the charge sequences. Generally, a fast expansion takes place, typically in $\tau_{ex} \sim 50\omega_{pe}^{-1}$. The radius that corresponds to Fig.5(a) makes slow amplitude oscillations between $R_g \sim 10a \pm 2a$ in the time period of $\sim 300\omega_{pe}^{-1}$. The velocity distribution functions for this case are anisotropic and deviating from the Maxwellian distribution, being consistent with large time variability of the conformation.

On the other hand, the gyration radius for the low temperature case $T/T_0 = 1/8$ decreases monotonically with the e-folding time $\tau_{rel} \sim 200\omega_{pe}^{-1}$, which is significantly slow compared to the expansion at high temperatures. When the number of the monomers is small ($N = 64$), the time history of the gyration radius shows the decrease in a similar time scale within some uncertainty originating from the randomness of the charge sequences. The relaxation time of the global structure appears to be independent of the number of the monomers on the chain. The equilibrium conformation thus reached is shown in Fig.5(b) which is spherical and compact. The velocity distribution functions for this case are nearly Maxwellian. During the collapse the chain becomes multiply folded; the distance between the connected monomers is shortened only a little. The charged monomers tend to be loosely aggregated to form neutral clusters, and the effective interaction is made through dipole component.

In order to eliminate aforementioned deviations originating from randomness of the charge sequences, multiple runs for the same set of the parameters are made starting from random conformations and charge sequences. Then, the results are averaged over these runs. Also, other series of the runs are performed for various values of the temperature, the exclusion length and the number of the monomers on the chain.

Figure 6 is the linear-scale plot of (a) the kinetic energy, (b) the electrostatic potential, (c) the connected-monomer distance, and (d) the gyration radius, for the 256-mer

polyampholyte chains with $a_{col} = 0.5a$, each of which is plotted against the temperature $T = e^2/a\Gamma$. Each point in the figure is the average over ten different runs. Energy equipartition is established between the kinetic and elastic energies over the wide temperature range; they are proportional to the temperature, $W_{kin} \sim W_{spr} \sim \frac{3}{2}T \propto \Gamma^{-1}$, due to the random thermal kicks and the frictional force exerted by the surrounding medium. However, there occurs a slight offset below the $\frac{3}{2}T$ line for the elastic energy at $T/T_0 < 1$. This is because the elastic energy, $W_{spr} = (3T/2a^2) < (\Delta r)^2 >$, is affected by contraction of the connected-monomer distance $(< (\Delta r)^2 >)^{1/2}$ in the low-temperature regime, especially at $T/T_0 < 0.5$. However, the decrease in the gyration radius is again much greater than that in the connected-monomer distance when the temperature is lowered. Folding of the chain is responsible for the global structural changes. Contraction of the connected-monomer distances adds up at low temperatures when the polyampholyte is very stiff, $v/a^3 \ll 1$.

The contraction of the connected-monomer distance is easily understood. When the Coulomb energy is negligible, the balance $\frac{3}{2}T \sim W_{spr}$ determines the distance as $< \Delta r > \sim a$. However, when $|\Phi| \geq W_{spr} \cong \frac{3}{2}T$, an addition of the restoring force between the positively and negatively charged monomer pair reduces the distance Δr. This is true for $T \leq T_0$ (or $\Gamma \geq 1$), as was shown in Fig.6(c). Alternatively, this is directly proven by omitting the Coulomb force and making the simulation runs in various temperatures; the connected monomer distance stays the same.

The magnitude of the electrostatic potential ($\Phi < 0$) increases as temperature is lowered, as depicted in Fig.6(b). This is consistent with reduction of the average monomer distance $2R_g/N^{1/3}$. The large-scale potential Φ_L defined below Eq.(9) is measured to be a fraction of the average potential Φ, but it stays negative (attractive) for the neutral polyampholytes. We note that the low and medium temperature regimes are characterized by $T \leq T_0$; the electrostatic potential equals or overcomes the kinetic energy. Especially for low temperatures, the Coulomb force stabilizes the neutral polyampholytes.

To obtain the precise functional form, the gyration radius for the $a_{col} = 0.5a$ cases is plotted in logarithmic scales against temperature and the number of monomers on the chain. The temperature dependence for the 64, 128 and 256-mers depicted in Fig.7 shows three

regimes in the temperature domain which are joined at $T/T_0 \sim 0.3$ and 1.0. The dependence on the number of monomers is plotted for the three temperature regimes in Fig.8. The functional form of the gyration radius is compiled to be, $R_g \sim N^{0.25}T^{0.8}$, $R_g \sim N^{0.33}T^{0.33}$, and $R_g \sim N^{0.5}$ in the low, medium and high temperature regimes, respectively. The electrostatic potential for the same series of the runs is depicted in Fig.9. There are again three regimes in the electrostatic potential which correspond to those in Fig.7. The change in the conformations between stretched, oblate and spherical ones are reflected in that of the electrostatic potential, thereby minimizing the free energy at each temperature regime. The electrostatic potential in the medium regime of Fig.9 is fitted by $|\Phi| \sim T^{-0.44}$, which is independent of the number of the monomers.

The gyration radius for the cases with the exclusion length $a_{col} = 0.2a$ is plotted also in logarithmic scales in Fig.10. Again, three regimes are identified, with the regime boundaries located this time at $T/T_0 \sim 0.8$ and 2.0, about twice greater than for the $a_{col} = 0.5a$ cases. The gyration radius is scaled as $R_g \sim N^{0.3}T^{1.0}$, $R_g \sim N^{0.4}T^{0.4}$, and $R_g \sim N^{0.6}$ in the low, medium and high temperature regimes, respectively. The electrostatic potential in the medium temperature regime is fitted by $|\Phi| \sim T^{-0.95}$. These dependences for the stiff chains are more sensitive to temperature than for the flexible chains.

When we compare the two series of the runs presented in Figs.7-10, it is found that the functional form of the gyration radius, $R_g \sim T^{\alpha}N^{\beta}$, is almost unique in the medium temperature regime, $\alpha \sim \beta \sim 1/3$. These values are not sensitive to the exclusion length or the number of the monomers for $N \geq 128$. The short chains with $N = 4^3$ seems to be somewhat different from the long chains probably because of comparatively large surface to volume ratio. For the "frozen state" in the low temperature regime, the exponent to temperature depends on the exclusion length, i.e. the stiffness of the polyampholytes. The exponents to temperature for the long chains ($N \geq 128$) are $\alpha \sim 0.8$ and 1.0 for $a_{col} = 0.5$ and $0.2a$, respectively. This tendency is qualitatively reasonable since the stiff polyampholyte with small exclusion radii can be more densely packed as the monomers come closer with each other at low temperatures.

A remarkable fact is that, although the temperatures for the regime boundaries de-

pends on the exclusion length, the gyration radius there becomes the same between different exclusion lengths if the number of the monomers is fixed (Table I). Furthermore, the regime boundaries are characterized by the unique values of the average monomer distance, $2R_g/N^{1/3}$, being independent of both the exclusion length and the number of the monomers on the chain, as depicted in the bottom part of Table I. The implications are, (i) the free energy of the polyampholyte is written mainly as the function of the average monomer distance, (ii) each conformation minimizes the free energy in that temperature regime through the electrostatic potential.

The high and medium temperature regimes identified in the molecular dynamics simulations correspond, respectively, to the unperturbed ($t > t_1$) and polyampholyte ($t < t_2$) regimes of the $\theta-$solvent of the Flory theory for which the second virial coefficient vanishes[10]. Indeed, for the charge neutral case, one has the spherical polyampholyte with its radius scaled as $R \sim N^{1/2}$ in the first regime, and the oblate polyampholyte with $R \sim (NT)^{1/3}$ in the second regime, in quantitatively good agreements with the analysis for Figs.7, 8 and 10. One difference is that the shape of the polyampholyte in the high temperature regime is stretched by molecular dynamics. But, since no principal axis exists as the shape is highly variable in time, the time average will result in the relation, $< L > \sim < D >$.

The previous Monte Carlo simulation with the lattice model[5] showed two regimes, the high and medium temperature regimes. But, the exponents to the temperature for the gyration radius and the electrostatic potential were appreciably small compared with the Flory theory and the long-chains of molecular dynamics simulations. For example, the gyration radius in the medium temperature regime was scaled as $R_{g,MC} \sim T^{0.20}$ instead of $R_{g,MD} \sim T^{1/3}$ for the molecular dynamics simulation (the long chains). Finally, the low temperature regime was not detected in the lattice model simulation as it incorporated the self-avoiding features of adjacent monomers and used the short chains $N \leq 64$.

(c) Reversibility under the Coulomb Force

The response of a single polyampholyte against successive temperature changes is studied in this subsection. We use a charge neutral, 64-mer chain with the exclusion length

$a_{col} = 0.2a$. The temperature is changed either slowly or rapidly in the following sequence: $T/T_0 = 2 \to 0.2 \to 2$ (i.e., $\Gamma = 0.5 \to 5 \to 0.5$).

Figure 11 depicts the time histories of the kinetic energy, the elastic energy, the gyration radius and the applied temperature from top to bottom, respectively. When the temperature is lowered and then raised quickly with the time constant $50\omega_{pe}^{-1}$ as in the left column, the kinetic and elastic energies follow the temperature change without time delay. But, the size of the polyampholyte does not follow the change immediately. The folding of the chain occurs rather slowly with the time constant $\tau_{rel} \sim 200\omega_{pe}^{-1}$ for the 64-mers; the expansion goes faster with $\tau_{ex} \sim 50\omega_{pe}^{-1}$. These are adiabatic time scales which are consistent with Sec.3(b).

On the other hand, when the temperature is changed gradually with the time constant $400\omega_{pe}^{-1}$ which is long compared with the relaxation time of the chain, the gyration radius of the polyampholyte closely follows the temperature change, as depicted in the right column of Fig.11. This simple experiment reveals that the conformation of the polyampholyte is exactly reversible under the Coulomb force (cf. Sec.4). The free energy has only one minimum with respect to the monomer separation.

4. Cooperation of Long and Short-Range Forces

It is known theoretically and by experiments that competition of the attractive and repulsive forces generates asymmetry in the phase transition[6]. Here, we reproduce such a process in the molecular dynamics simulation by introducing the second local minimum to the free energy. The short-range attractive force that corresponds to a negative value of the second virial coefficient $B < 0$ (poor solvent) may be modeled by the force that operates between the two monomers placed within a certain distance,

$$\mathbf{F}_{SR}(\mathbf{r}) = \begin{cases} -f_0\hat{\mathbf{r}} & \text{for} \quad r < a_{SR}, \\ 0 & \text{otherwise.} \end{cases} \tag{10}$$

Including the Coulomb force and the short-range force given by Eq.(3) and (10), molecular dynamics simulations are performed.

Figure 12 depicts the time histories of the gyration radius and corresponding final conformations of the 64-mer neutral polyampholyte chains for (a) the force constant $f_0 = 10$, (b) $f_0 = 15$, and (c) $f_0 = 15$ without the Coulomb force. Other parameters are $a_{SR} = 0.5a$, $a_{col} = 0.2a$ and $T/T_0 = 1$. The figure shows that the equilibrium conformation is not affected by the short-range force when the force is weak, $f_0 < f_0^{crit} \sim 13$. Otherwise for case (b), the gyration radius decreases from $R_g \sim 3a$ to $1.2a$ in the time interval of $\tau \sim 50\omega_{pe}^{-1}$. The attractive force results in a compact conformation when it dominates over the Coulomb force at the short range $r \leq a_{SR}$. On the other hand, when the long-range force is omitted, the reduction of the radius still occurs but slowly in $\tau \sim 100\omega_{pe}^{-1}$ as shown in Fig.12(c). Thus, cooperation of the Coulomb force and the short-range force is nonlinearly additive such that the Coulomb force brings the monomers to a short distance where the short-range force is operative. The time constant of the collapse is expected to be progressively extended as the range of the force a_{SR} is reduced.

The observation that the size of the polyampholyte is drastically reduced by addition of the short-range force implies that there will be a hysteresis against successive temperature changes under the long and short-range forces. In the following run, the temperature is raised gradually in $\tau = 1000\omega_{pe}^{-1}$ as $T/T_0 = 1 \rightarrow 2$ in the first stage, and is then lowered to the initial value $T/T_0 = 2 \rightarrow 1$ in the second stage (Fig.13). During this operation, the size of the polyampholyte increases suddenly at $T \sim 1.4T_0$ in the first stage as shown in the right column of Fig.13. Both the volume and the gyration radius undergo amplitude oscillations around $< V > \sim 32a^3$ and $R_g \sim 4a$. The polyampholyte once expanded maintains such a conformation until the temperature falls down to $T \sim 1.1T_0$ in the second stage. The shrink process occurs in a short time interval. The final gyration radius thus reached is the same as the initial one.

The above transition process invoked by the temperature change is plotted as the (T, R_g) diagram in the left column of Fig.13. The data points are sampled in every $50\omega_{pe}^{-1}$ for $t \geq 200\omega_{pe}^{-1}$ and are processed with broad-window smoothing of $300\omega_{pe}^{-1}$ for the expanded phase. A hysteresis of the transition path is seen in the figure. More precisely, when the temperature is raised, the transition path takes the lower branch rightward starting at

$(T_0, 1.2a)$ and jumps up to $R_g \sim 3a$ at $T \sim 1.4T_0$; in the reverse way, the path takes the upper branch leftward and then steps down abruptly as $R_g \sim 3a \rightarrow 1.2a$ at $T \sim 1.1T_0$.

It is remarked that this transition temperature is unique for the given set of parameters of a_{SR}, a_{col} and f_0; the temperature at which the collapse occurs in the second stage does not change when the temperature is lowered twice more rapidly. The hysteresis of the transition path which is caused by the cooperation of the long and short-range forces is clearly contrasted to the exactly reversible process under the Coulomb force only (Sec.3(c)).

5. Conclusion

Using the molecular dynamics simulation technique, we studied in this paper the dynamical evolution and the equilibrium properties of the polyampholytes in terms of charge imbalance, temperature, length and stiffness of the chain. The polyampholytes submerged in the viscous medium evolved following the Eqs.(1)-(3) while receiving random thermal kicks and the frictional force. The major observations under the Coulomb interactions (I) and the Coulomb and short-range forces (II) were as follows:

(I.a) The equilibrium conformation was stretched and oscillating in time when the amount of charge imbalance exceeded $N^{1/2}$, for which the large-scale potential was positive (repulsive). The oscillation period of the gyration radius, i.e., the size of the polyampholyte, is proportional to the total length (mass) of the chain.

(I.b) Three regimes with different conformations and parameter dependences were identified in the temperature domain under the Coulomb force. The polyampholyte was spherical, oblate and stretched in the low, medium and high temperature regimes, respectively. The change in the conformations minimized the free energy of each regime through the electrstatic potential. The gyration radius was scaled as $R_g \sim N^{0.3}T^{0.8-1.0}$, $(NT)^{1/3}$, and $N^{1/2}$. The regime boundaries were characterized by the unique values of the monomer distance $2R_g/N^{1/3}$, although the stiffness of the chain affected the transition temperatures across the regime boundaries.

(I.c) The polyampholyte relaxed to the equilibrium conformation in $\tau_{rel} = 200 \sim 300\omega_{pe}^{-1}$

(e-folding time) due to folding of the chain at low temperature. The expansion of the polyampholyte took place more rapidly in $\tau_{ex} \sim 50\omega_{pe}^{-1}$ for high temperatures. The relaxation time of the global structure was independent of the number of the monomers on the chain. Under the Coulomb force, the transition among the different regimes was exactly reversible with temperature.

(II) The cooperation of the short-range and Coulomb forces acted to organize the structure of the polyampholyte. A compact conformation was obtained even above the normal transition temperature across the regime boundary. Hysteresis of the phase transition path against successive temperature changes was demonstrated.

The "frozen state" for low temperatures summarized in (I.b) was identified for the first time, owing to the molecular dynamics simulation which allowed densely-packed conformations in the configuration space, unlike the lattice model. However, this frozen state may not necessarily occur for all the polymers, especially for those associated with large side chains.

The cooperation of the short and long-range forces was a nonlinear superposition of the forces, as the long-range Coulomb force brought the monomers to short distances where the short-range force was operative.

In the molecular dynamics simulations, the evolution of the polyampholytes was traced in time by integrating the Newton's equations of motion with a finite time step Δt. The range of the temperature that was suitable for the molecular dynamics was rather limited, $0.1 \leq T/T_0 \leq 3$, due to the necessity of a small time step for $T/T_0 \gg 3$, and the numerical fluctuations associated with dynamical motions of the monomers for $T/T_0 \ll 0.1$.

Nevertheless, good agreements were found between the molecular dynamics simulations and the θ-solvent of the Flory theory of the polyampholytes. Namely, (i) stretched conformations were obtained for the non-neutral polyampholyte with $\delta N > N^{1/2}$, (ii) the high and medium temperature regimes were identified with the correct scaling for the gyration radius, (iii) the transition among the different regimes of the polyampholyte showed hysteresis, as predicted when the attractive and repulsive forces coexist.

However, qualitative and quantitative differences were found between the present study and the Monte Carlo simulation, especially in the temperature dependence of the gyration radius and the Coulomb potential. This was attributable to that the densely-packed states of the stiff polyampholytes ($v/a^3 \ll 1$) are better treated by the molecular dynamics simulation than with the lattice model adopted in the Monte Carlo simulation. The molecular dynamics simulation allows the monomers to occupy any point in the phase space unless prohibited explicitly by the potential function. By contrast, the lattice model which was useful in modeling the exclusion effects of large side chains of the polymers restricted the number, direction and distance of the close neighbor monomers to those allowed by vertices of the cubic lattice. It is emphasized that the choice of the stiffness parameter in our study, v/a^3, is in good accordance with the real laboratory and biological polymers.

Acknowledgments

It is a great pleasure for one of the authors (M.T.) to thank Professor Bruno Coppi who hosted him to make a sabbatical research at the Massachusetts Institute of Technology (MIT) during the year 1996-97. His research at MIT was mainly supported by the grant from Japan Society for the Promotion of Science.

References

1. J.H.Chu and I.Lin, Phys.Rev.Lett., 72, 4009 (1994).
2. H.Hora, Plasmas at High Temperature and Density (Springer, Berlin, 1991).
3. S.Ogata, H.Iyetomi, S.Ichimaru, and H.M.Van Horn, Phys.Rev.E, 48, 1344 (1993).
4. C.Tanford, Physical Chemistry of Macromolecules (Willey, New York, 1961).
5. Y.Kantor, M.Kardar and H.Li, Phys.Rev.E, 49, 1383 (1994).
6. T.Tanaka, S-T.Sun, Y.Hirokawa, S.Katayama, J.Kucera, Y.Hirose, and T.Amiya, Nature, 325, 796 (1987).
7. J.A.McCammon and S.C.Harvey, Dynamics of Proteins and Nucleic Acids (Cambridge University Press, Cambridge, 1987).
8. A.Y.Grosberg and A.R.Khokhlov, Statistical Physics of Macromolecules (AIP Press, New York, 1994).
9. S.Ichimaru, Basic Principles of Plasma Physics (Benjamin, Reading, 1973).
10. A.V.Dobrynin and M.Rubinstein, J.Phys.II France, 5, 677 (1995).
11. M.Tanaka, T.Tanaka, V.S.Pande, and A.Y.Grosberg, Bull.Amer.Phys.Soc., 41, 1522 (1996).

Table I: The characteristic value of the temperature T, the gyration radius R_g, and the average monomer distance $2R_g/N^{1/3}$ at the boundary of the low and medium temperature regimes (L-M), and of the medium and high temperature regimes (M-H).

	L-M	M-H	Remarks
T	$0.3T_0$	$1.0T_0$	$a_{col} = 0.5a, N = 256$
	$0.8T_0$	$2.0T_0$	$a_{col} = 0.2a, N = 256$
R_g	$6a$	$8.6a$	$a_{col} = (0.2a, 0.5a), N = 256$
$2R_g/N^{1/3}$	$1.9a$	$2.7a$	$N = 256$
	$2.0a$	$2.7a$	$N = 64$

Figure Captions

Figure 1. The time sequential plots of the 256-mer polyampholyte chain at (a) $t = 0$, (b) $t = 50\omega_{pe}^{-1}$, and (c) $t = 600\omega_{pe}^{-1}$ of molecular dynamics simulation. The parameters are $T = \frac{1}{2}T_0$, $a_{col} = 0.2a$, and the charge imbalance is 1.6%. The (+) and dot on the chain represent positive and negative monomers, respectively.

Figure 2. The time histories of (a) the kinetic energy, (b) the elastic energy, (c) the electrostatic potential, and (d) the gyration radius of the polyampholyte shown in Fig.1.

Figure 3. The equilibrium conformations and the time histories of the gyration radius for the 256-mer chains with $a_{col} = 0.2a$ and $T = \frac{1}{2}T_0$. The charge imbalance is (a) $\delta N/N =$ 1.6%, (b) 6.3%, and (c) 14.1%. The conformation for (c) is reduced to 53% that of the original one.

Figure 4. (a) The case distribution of non-neutral 64-mer chains against the charge imbalance. The equilibrium values of (b) the gyration radius, (c) the connected monomer distance, and (d) the elastic energy against charge imbalance. The parameters are $T/T_0 = 1/5$ and $a_{col} = 0.5a$.

Figure 5. The equilibrium conformations of the neutral 256-mer chains with $a_{col} = 0.5a$, and corresponding velocity distribution functions in the x, y, z-directions for (a) $T/T_0 = 2$ and (b) $T/T_0 = 1/8$. The maximum and minimum of the velocity plots are six times the thermal speed.

Figure 6. The temperature dependence of (a) the kinetic energy, (b) the electrostatic potential, (c) the connected-monomer distance, and (d) the gyration radius of the neutral 256-mers with $a_{col} = 0.5a$.

Figure 7. The temperature dependence of the gyration radius in logarithmic scales for the neutral 64, 128 and 256-mer polyampholytes with $a_{col} = 0.5a$. Three different regimes are identified at low, meduim and high temperatures.

Figure 8. The dependence of the gyration radius on the number of monomers on the chain in logarithmic scales at $T/T_0 = 0.2$, 0.5 and 2.0 for the neutral polyampholytes with $a_{col} = 0.5a$.

Figure 9. The magnitude of the electrostatic potential $|\Phi|$ against temperature in logarithmic scales for the polyampholytes depicted in Fig.7. Three regimes are again identified at low, meduim and high temperatures.

Figure 10. The temperature dependence of the gyration radius in logarithmic scales for the neutral 64, 128 and 256-mer polyampholytes with $a_{col} = 0.2a$.

Figure 11. The time histories of the kinetic energy, the elastic energy, the gyration radius, and the applied temperature, from top to bottom in this order. The left and right columns correspond to rapid and slow temperature changes, respectively.

Figure 12. The equilibrium conformations and the time history of the gyration radius for (a) the force constant $f_0 = 10$, (b) $f_0 = 15$, and (c) $f_0 = 15$ without the Coulomb force.

Figure 13. The diagram of the gyration radius versus temperature for a single 64-mer polyampholyte under the Coulomb and short-range forces in the left column. The time histories of the volume, the gyration radius, and the applied temperature for the same run, from top to bottom in the right column.

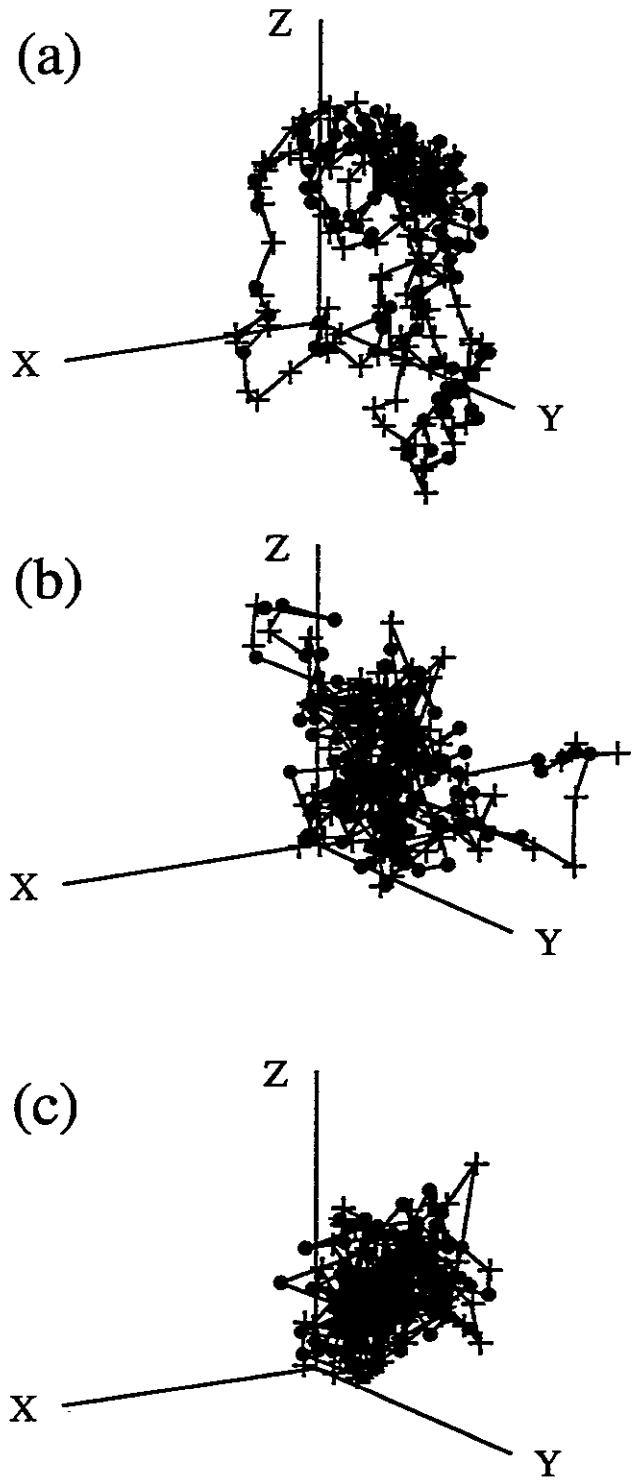

FIG.1

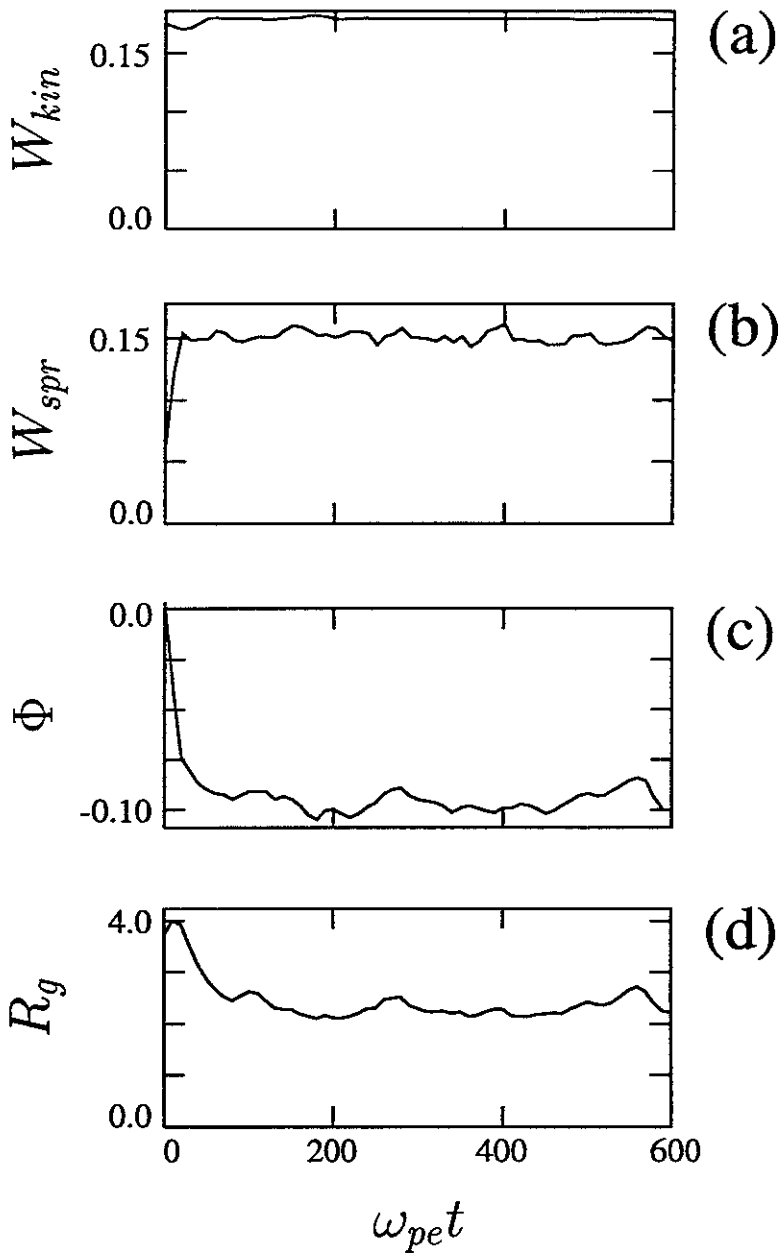
(a)
W_{kin}
0.15
0.0
(b)
W_{spr}
0.15
0.0
(c)
Φ
0.0
-0.10
(d)
R_g
4.0
0.0
0
200
400
600
$\omega_{pe}t$

FIG.2

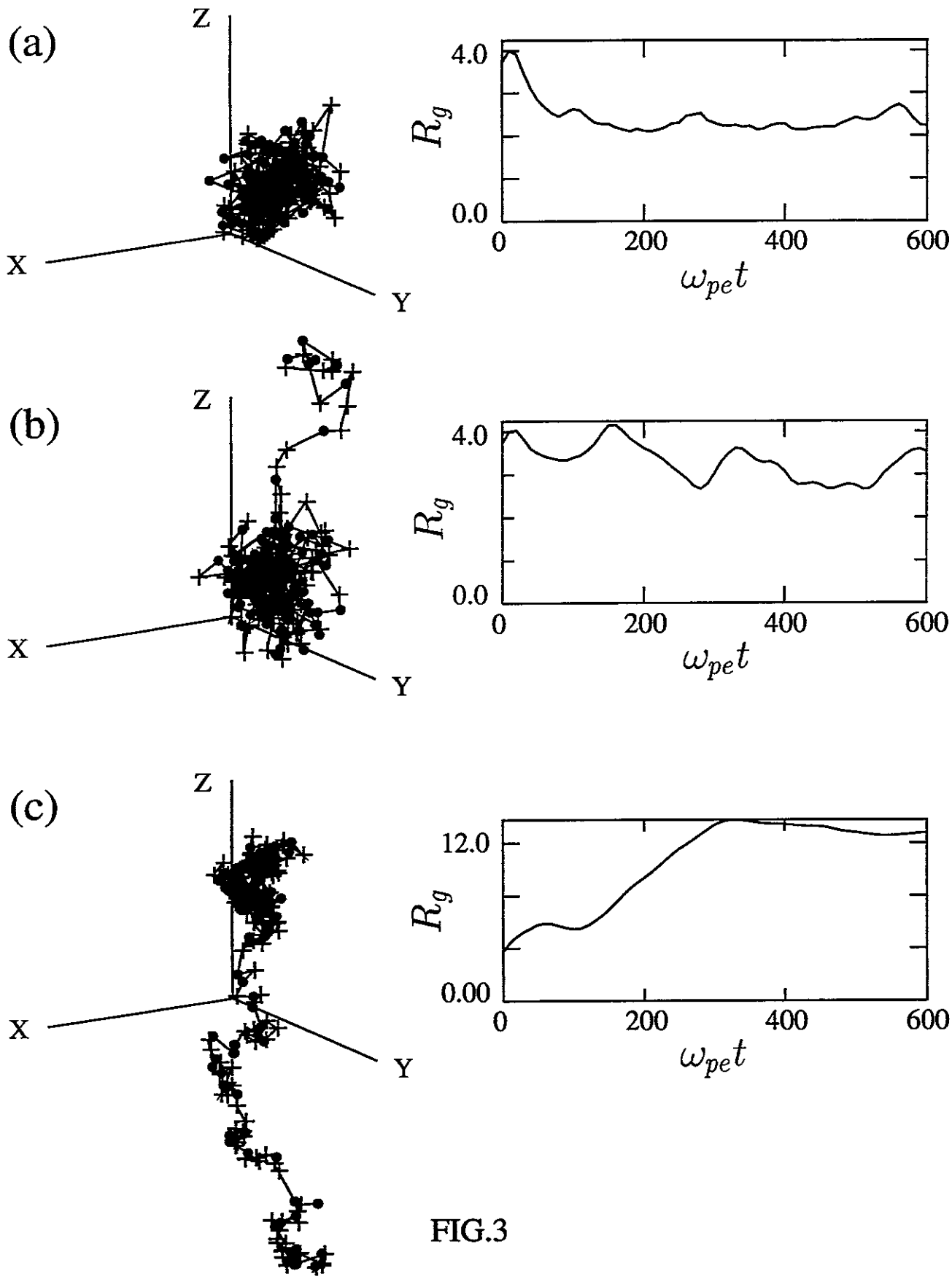
(a)
Z
X
Y
4.0
0.0
R_g
0
200
400
600
$\omega_{pe}t$
(b)
Z
X
Y
4.0
0.0
R_g
0
200
400
600
$\omega_{pe}t$
(c)
Z
X
Y
12.0
0.00
R_g
0
200
400
600
$\omega_{pe}t$

FIG.3

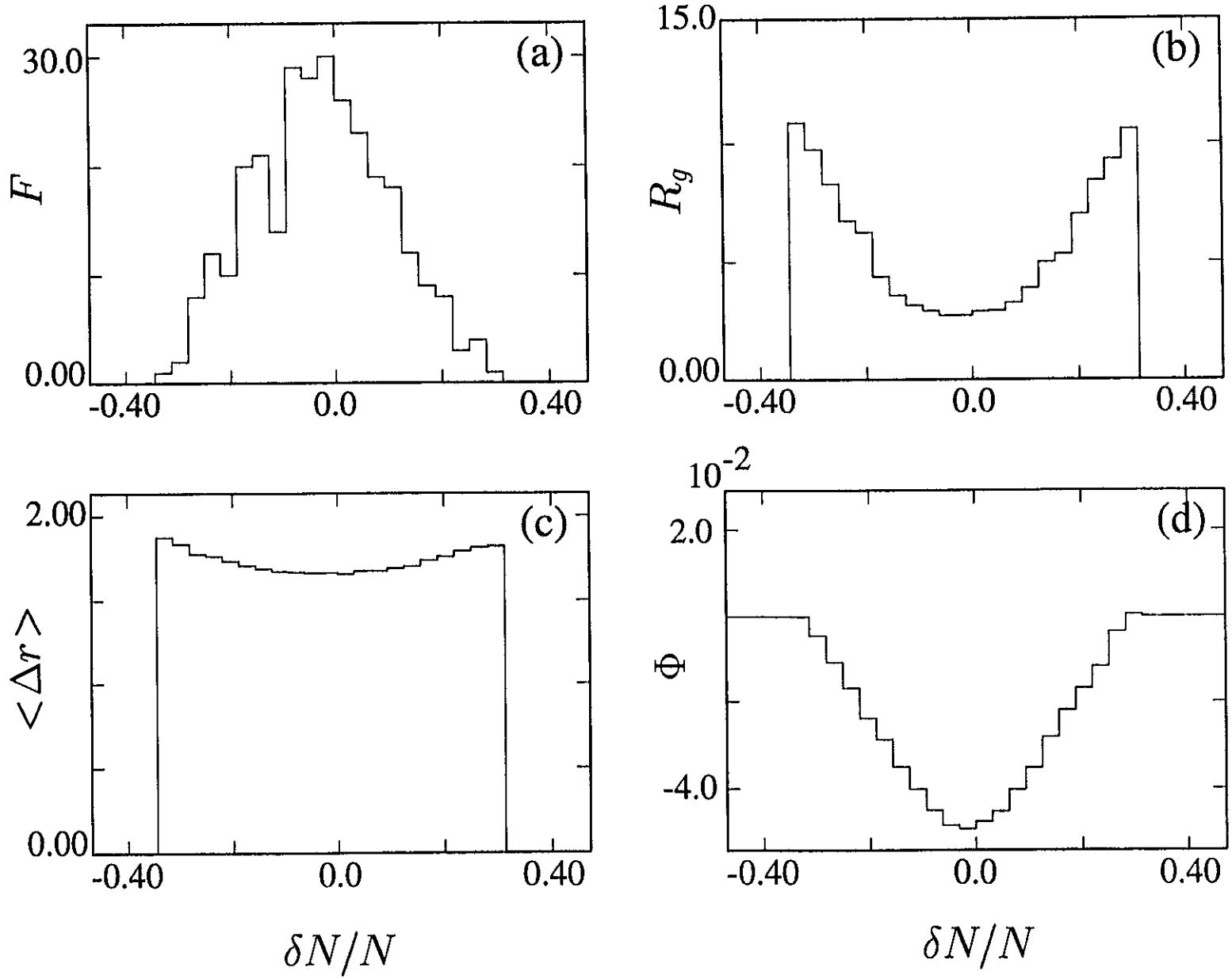
(a)
30.0
0.00
F
-0.40
0.0
0.40
(b)
15.0
0.00
R_g
-0.40
0.0
0.40
(c)
2.00
0.00
$<\Delta r>$
-0.40
0.0
0.40
$\delta N/N$
(d)
10^{-2}
2.0
-4.0
Φ
-0.40
0.0
0.40
$\delta N/N$

FIG.4

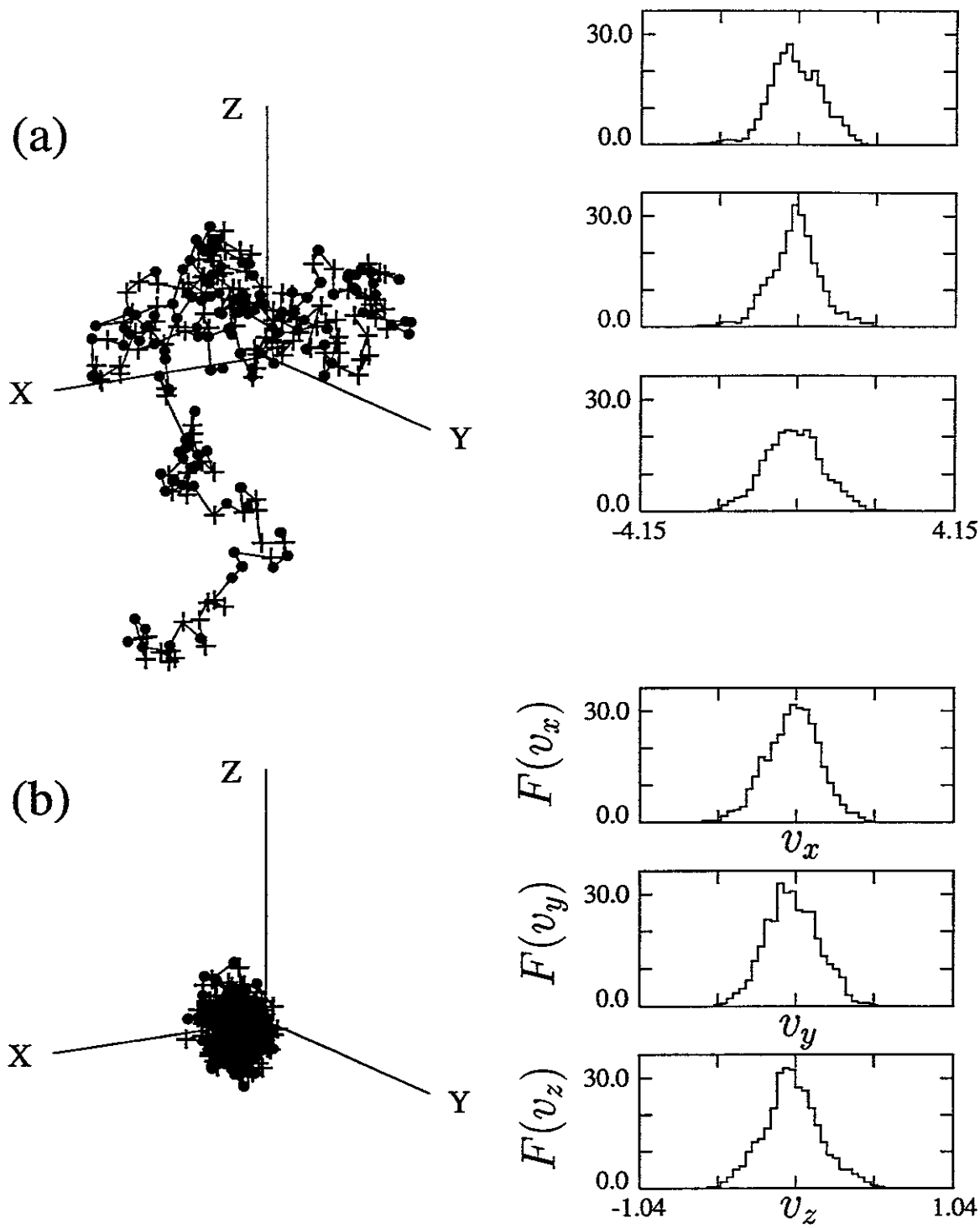
(a)
Z
X
Y
30.0
0.0
30.0
0.0
30.0
0.0
-4.15
4.15
(b)
Z
X
Y
$F(v_x)$
30.0
0.0
v_x
$F(v_y)$
30.0
0.0
v_y
$F(v_z)$
30.0
0.0
-1.04
v_z
1.04

FIG.5

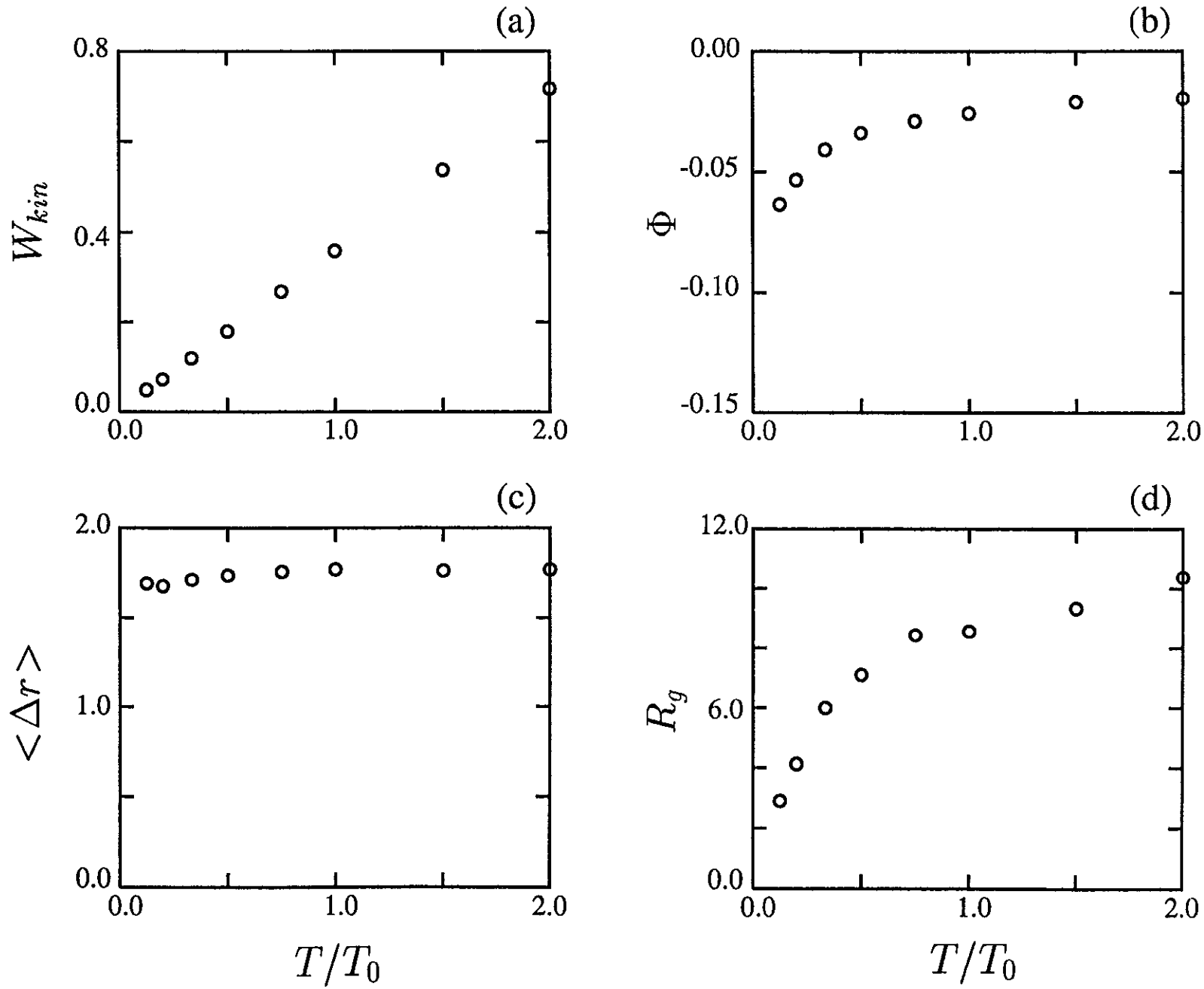
(a)
0.8
0.4
0.0
W_{kin}
0.0
1.0
2.0
(b)
0.00
-0.05
-0.10
-0.15
Φ
0.0
1.0
2.0
(c)
2.0
1.0
0.0
$<\Delta r>$
0.0
1.0
2.0
T/T_0
(d)
12.0
6.0
0.0
R_g
0.0
1.0
2.0
T/T_0

FIG.6

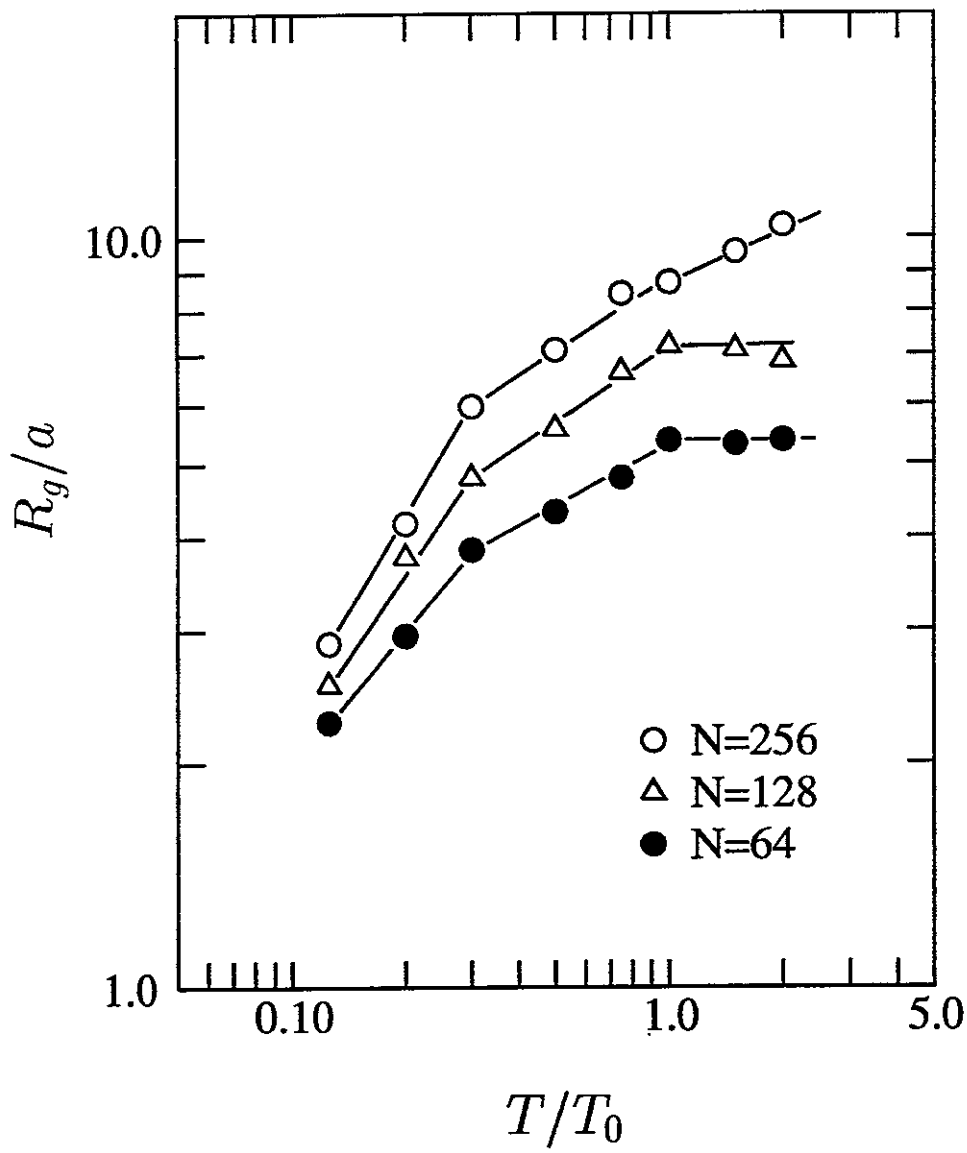

FIG.7

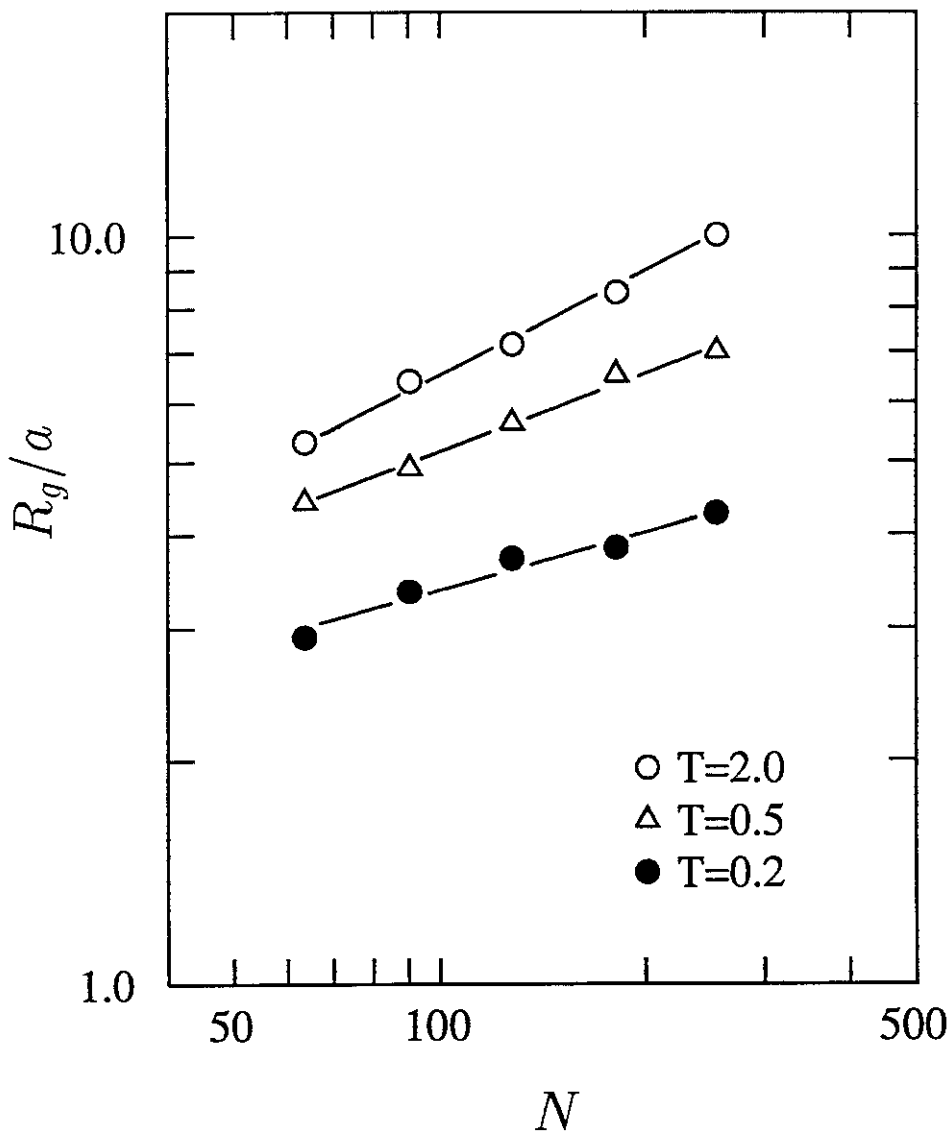

FIG.8

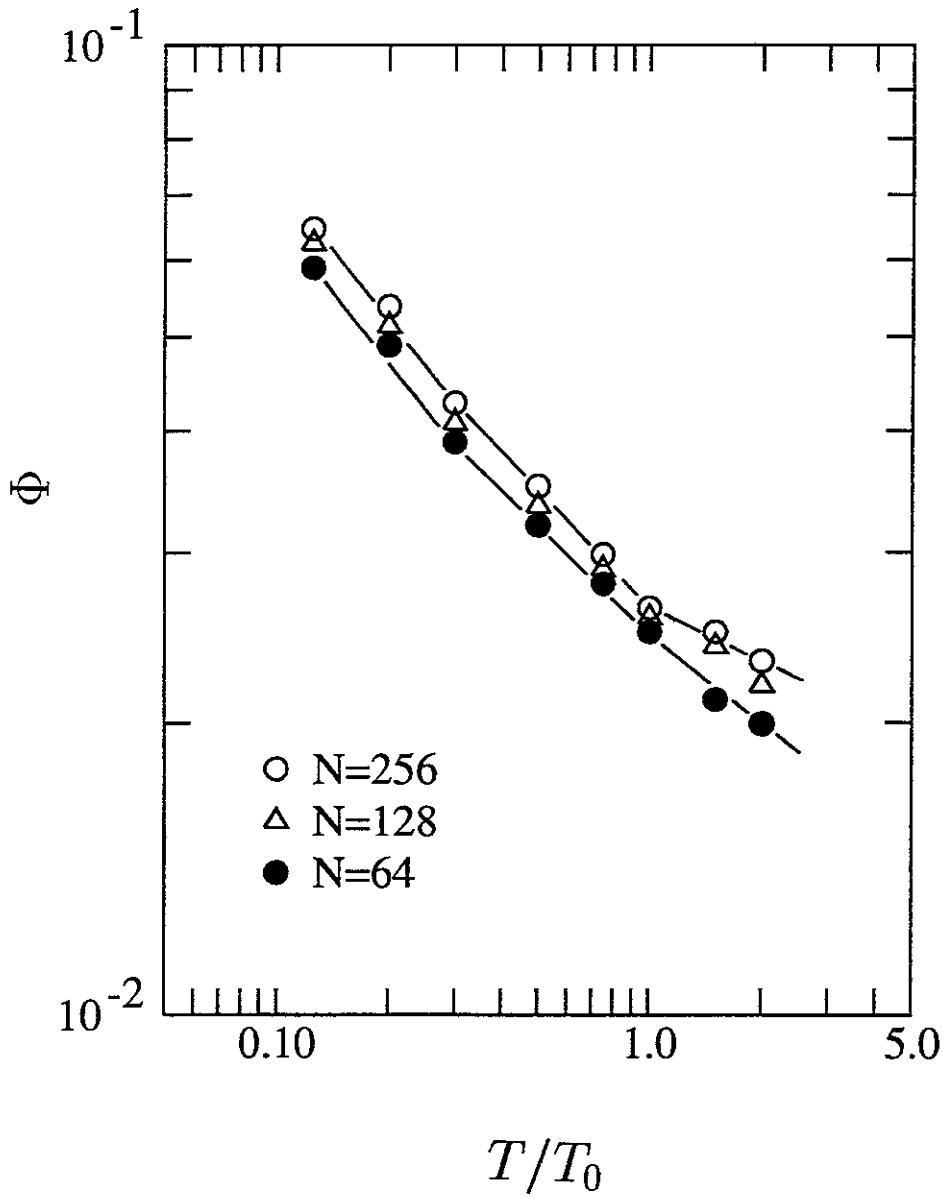

FIG.9

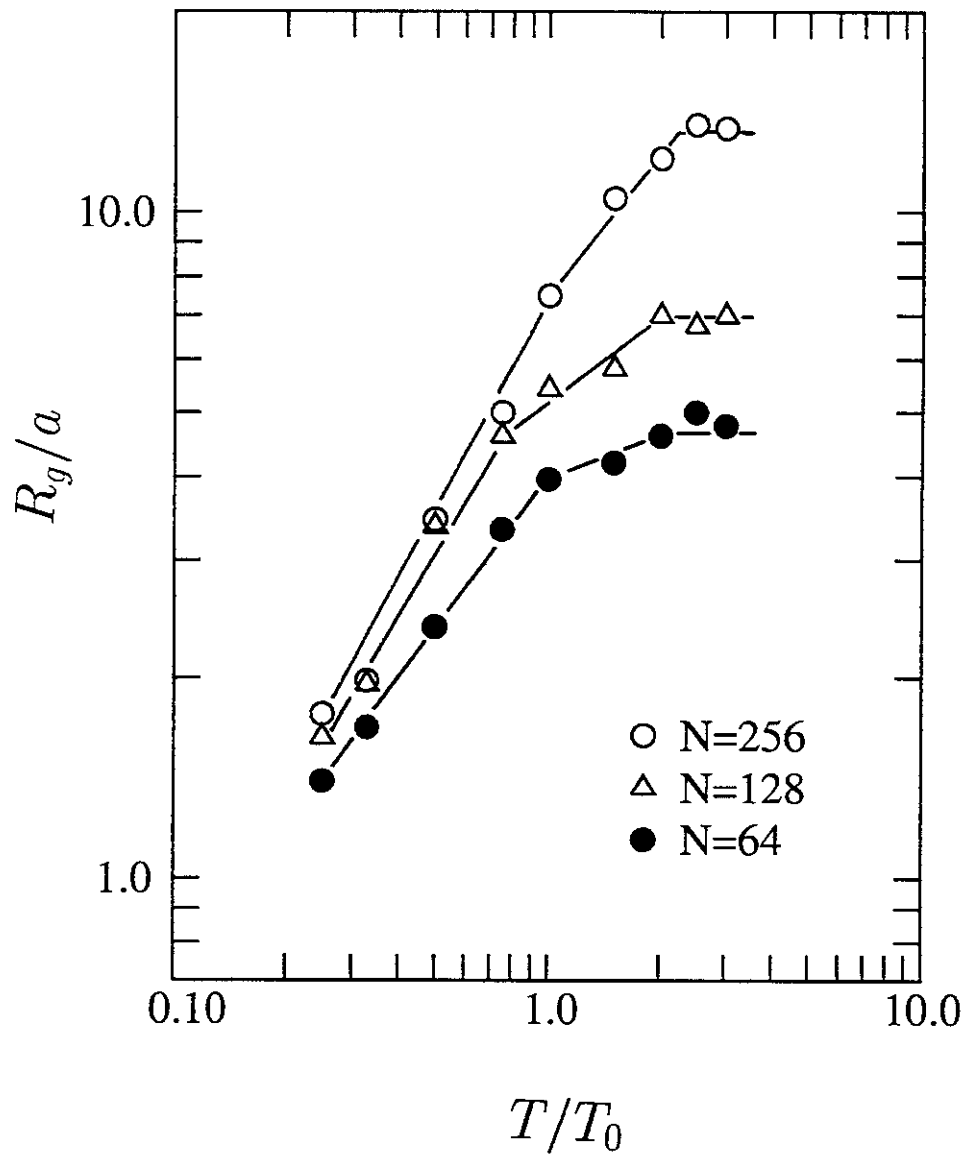

FIG.10

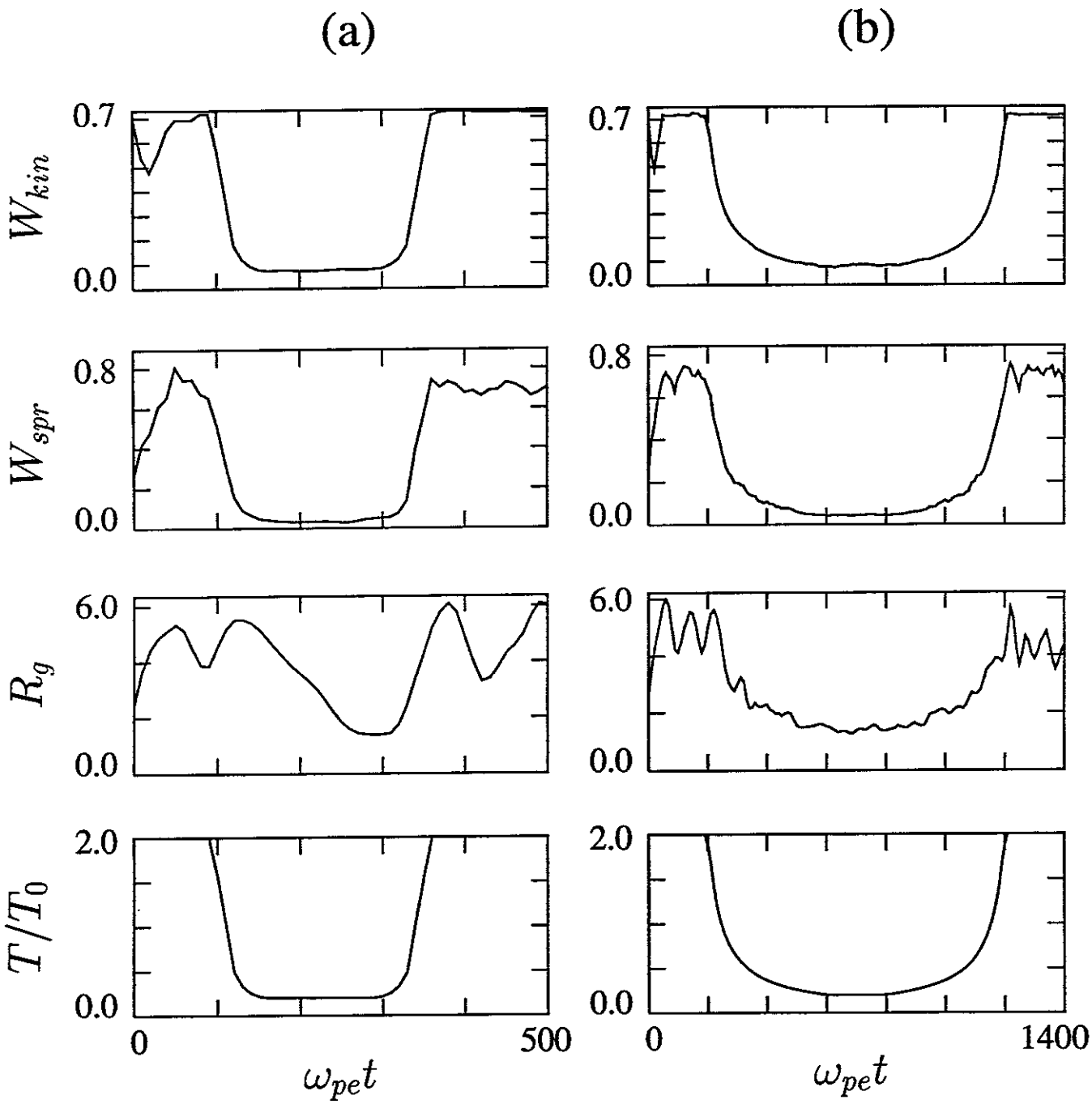

FIG.11

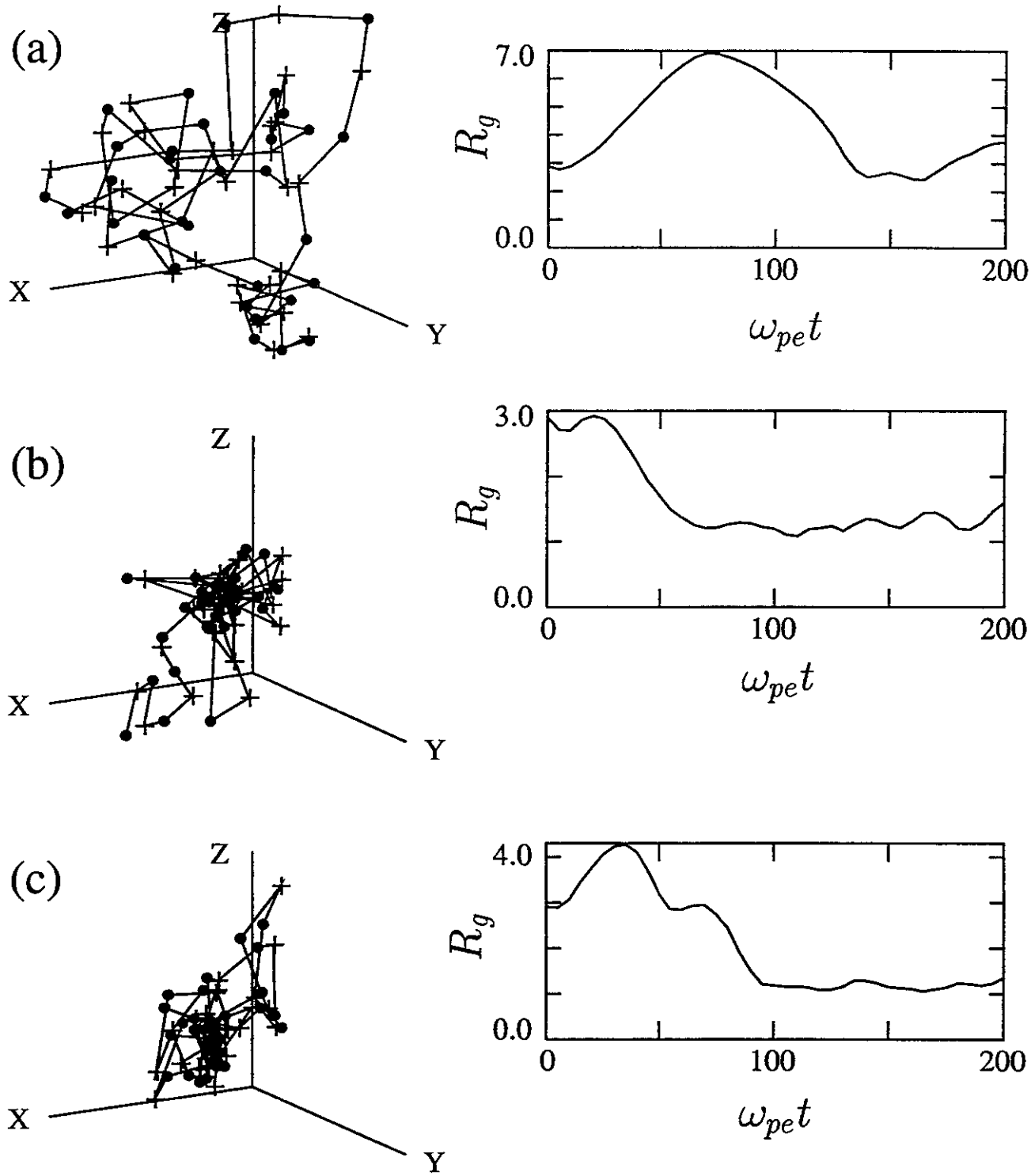
(a)
Z
X
Y
7.0
0.0
R_g
0
100
200
$\omega_{pe}t$
(b)
Z
X
Y
3.0
0.0
R_g
0
100
200
$\omega_{pe}t$
(c)
Z
X
Y
4.0
0.0
R_g
0
100
200
$\omega_{pe}t$

FIG.12

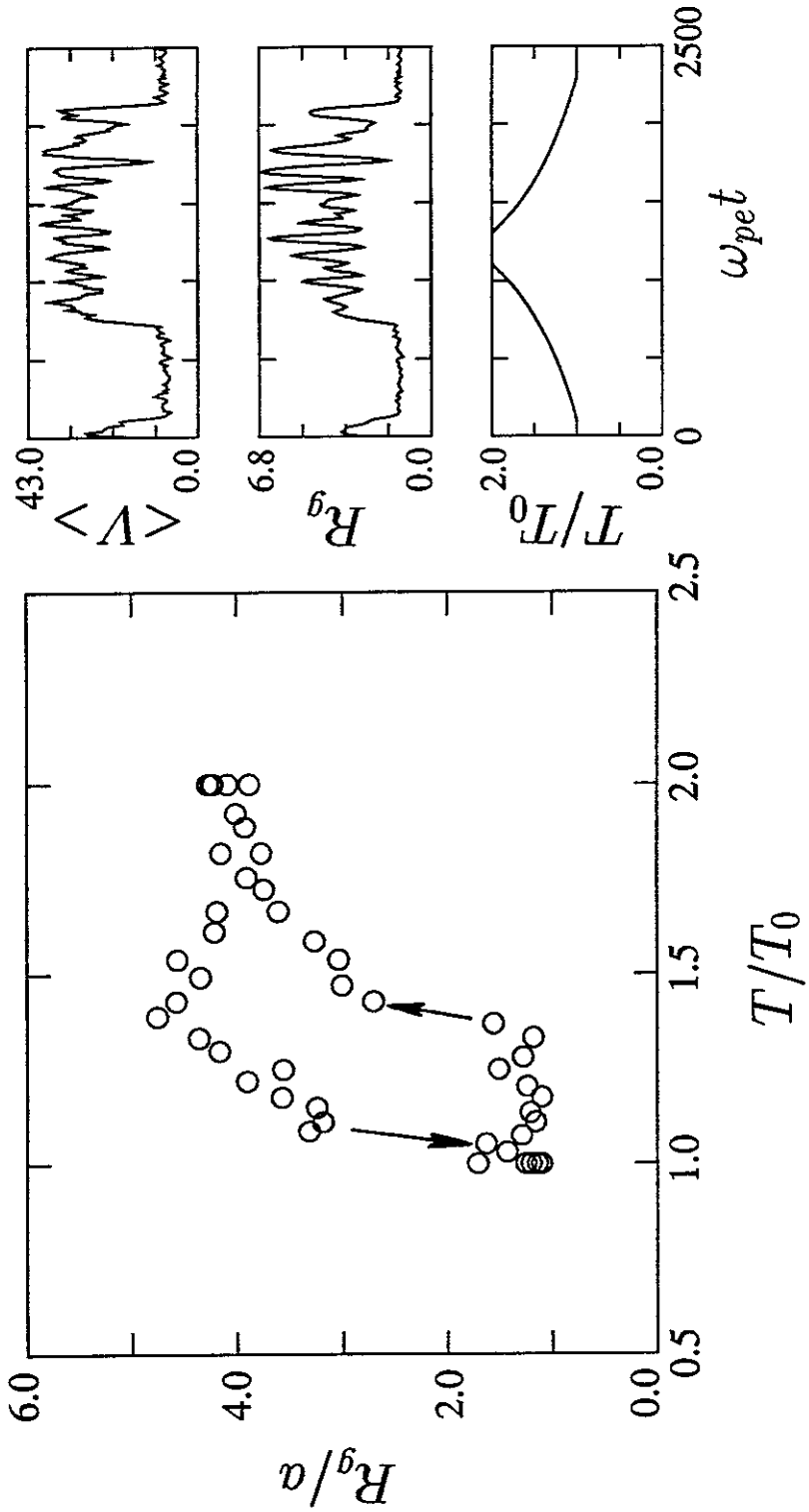

FIG.13

Recent Issues of NIFS Series

NIFS-452 N. Nakajima, K. Ichiguchi, M. Okamoto and R.L. Dewar,
Ballooning Modes in Heliotrons/Torsatrons; Sep. 1996 (IAEA-CN-64/D3-6)

NIFS-453 A. Iiyoshi,
Overview of Helical Systems; Sep. 1996 (IAEA-CN-64/O1-7)

NIFS-454 S. Saito, Y. Nomura, K. Hirose and Y.H. Ichikawa,
Separatrix Reconnection and Periodic Orbit Annihilation in the Harper Map; Oct. 1996

NIFS-455 K. Ichiguchi, N. Nakajima and M. Okamoto,
Topics on MHD Equilibrium and Stability in Heliotron / Torsatron; Oct. 1996

NIFS-456 G. Kawahara, S. Kida, M. Tanaka and S. Yanase,
Wrap, Tilt and Stretch of Vorticity Lines around a Strong Straight Vortex Tube in a Simple Shear Flow; Oct. 1996

NIFS-457 K. Itoh, S.- I. Itoh, A. Fukuyama and M. Yagi,
Turbulent Transport and Structural Transition in Confined Plasmas; Oct. 1996

NIFS-458 A. Kageyama and T. Sato,
Generation Mechanism of a Dipole Field by a Magnetohydrodynamic Dynamo; Oct. 1996

NIFS-459 K. Araki, J. Mizushima and S. Yanase,
The Non-axisymmetric Instability of the Wide-Gap Spherical Couette Flow; Oct. 1996

NIFS-460 Y. Hamada, A. Fujisawa, H. Iguchi, A. Nishizawa and Y. Kawasumi,
A Tandem Parallel Plate Analyzer; Nov. 1996

NIFS-461 Y. Hamada, A. Nishizawa, Y. Kawasumi, A. Fujisawa, K. Narihara, K. Ida, A. Ejiri, S. Ohdachi, K. Kawahata, K. Toi, K. Sato, T. Seki, H. Iguchi, K. Adachi, S. Hidekuma, S.Hirokura, K. Iwasaki, T. Ido, M. Kojima, J. Koong, R. Kumazawa, H. Kuramoto, T. Minami, I. Nomura, H. Sakakita, M. Sasao, K.N. Sato, T. Tsuzuki, J. Xu, I. Yamada and T. Watari,
Density Fluctuation in JIPP T-IIU Tokamak Plasmas Measured by a Heavy Ion Beam Probe; Nov. 1996

NIFS-462 N. Katsuragawa, H. Hojo and A. Mase,
Simulation Study on Cross Polarization Scattering of Ultrashort-Pulse Electromagnetic Waves; Nov. 1996

NIFS-463 V. Voitsenya, V. Konovalov, O. Motojima, K. Narihara, M. Becker and B. Schunke,
Evaluations of Different Metals for Manufacturing Mirrors of Thomson

Scattering System for the LHD Divertor Plasma; Nov. 1996

NIFS-464 M. Pereyaslavets, M. Sato, T. Shimozuma, Y. Takita, H. Idei, S. Kubo, K. Ohkubo and K. Hayashi,
Development and Simulation of RF Components for High Power Millimeter Wave Gyrotrons; Nov. 1996

NIFS-465 V.S. Voitsenya, S. Masuzaki, O. Motojima, N. Noda and N. Ohyabu,
On the Use of CX Atom Analyzer for Study Characteristics of Ion Component in a LHD Divertor Plasma; Dec. 1996

NIFS-466 H. Miura and S. Kida,
Identification of Tubular Vortices in Complex Flows; Dec. 1996

NIFS-467 Y. Takeiri, Y. Oka, M. Osakabe, K. Tsumori, O. Kaneko, T. Takanashi, E. Asano, T. Kawamoto, R. Akiyama and T. Kuroda,
Suppression of Accelerated Electrons in a High-current Large Negative Ion Source; Dec. 1996

NIFS-468 A. Sagara, Y. Hasegawa, K. Tsuzuki, N. Inoue, H. Suzuki, T. Morisaki, N. Noda, O. Motojima. S. Okamura, K. Matsuoka, R. Akiyama, K. Ida, H. Idei, K. Iwasaki, S. Kubo, T. Minami, S. Morita, K. Narihara, T. Ozaki, K. Sato, C. Takahashi, K. Tanaka, K. Toi and I. Yamada,
Real Time Boronization Experiments in CHS and Scaling for LHD; Dec. 1996

NIFS-469 V.L. Vdovin, T.Watari and A. Fukuyama,
3D Maxwell-Vlasov Boundary Value Problem Solution in Stellarator Geometry in Ion Cyclotron Frequency Range (final report); Dec. 1996

NIFS-470 N. Nakajima, M. Yokoyama, M. Okamoto and J. Nührenberg,
Optimization of M=2 Stellarator; Dec. 1996

NIFS-471 A. Fujisawa, H. Iguchi, S. Lee and Y. Hamada,
Effects of Horizontal Injection Angle Displacements on Energy Measurements with Parallel Plate Energy Analyzer; Dec. 1996

NIFS-472 R. Kanno, N. Nakajima, H. Sugama, M. Okamoto and Y. Ogawa,
Effects of Finite-β and Radial Electric Fields on Neoclassical Transport in the Large Helical Device; Jan. 1997

NIFS-473 S. Murakami, N. Nakajima, U. Gasparino and M. Okamoto,
Simulation Study of Radial Electric Field in CHS and LHD; Jan. 1997

NIFS-474 K. Ohkubo, S. Kubo, H. Idei, M. Sato, T. Shimozuma and Y. Takita,
Coupling of Tilting Gaussian Beam with Hybrid Mode in the Corrugated Waveguide; Jan. 1997

NIFS-475 A. Fujisawa, H. Iguchi, S. Lee and Y. Hamada,
Consideration of Fluctuation in Secondary Beam Intensity of Heavy Ion

Beam Prove Measurements; Jan 1997

NIFS-476 Y. Takeiri, M. Osakabe, Y. Oka, K. Tsumori, O. Kaneko, T. Takanashi, E. Asano, T. Kawamoto, R. Akiyama and T. Kuroda,
Long-pulse Operation of a Cesium-Seeded High-Current Large Negative Ion Source; Jan. 1997

NIFS-477 H. Kuramoto, K. Toi, N. Haraki, K. Sato, J. Xu, A. Ejiri, K. Narihara, T. Seki, S. Ohdachi, K Adati, R. Akiyama, Y. Hamada, S. Hirokura, K. Kawahata and M. Kojima,
Study of Toroidal Current Penetration during Current Ramp in JIPP T-IIU with Fast Response Zeeman Polarimeter; Jan., 1997

NIFS-478 H. Sugama and W. Horton,
Neoclassical Electron and Ion Transport in Toroidally Rotating Plasmas; Jan. 1997

NIFS-479 V.L. Vdovin and I.V. Kamenskij,
3D Electromagnetic Theory of ICRF Multi Port Multi Loop Antenna; Jan. 1997

NIFS-480 W.X. Wang, M. Okamoto, N. Nakajima, S Murakami and N. Ohyabu,
Cooling Effect of Secondary Electrons in the High Temperature Divertor Operation; Feb. 1997

NIFS-481 K. Itoh, S.-I. Itoh, H. Soltwisch and H.R. Koslowski,
Generation of Toroidal Current Sheet at Sawtooth Crash; Feb. 1997

NIFS-482 K. Ichiguchi,
Collisionality Dependence of Mercier Stability in LHD Equilibria with Bootstrap Currents; Feb. 1997

NIFS-483 S. Fujiwara and T. Sato,
Molecular Dynamics Simulations of Structural Formation of a Single Polymer Chain: Bond-orientational Order and Conformational Defects; Feb. 1997

NIFS-484 T. Ohkawa,
Reduction of Turbulence by Sheared Toroidal Flow on a Flux Surface; Feb. 1997

NIFS-485 K. Narihara, K. Toi, Y. Hamada, K. Yamauchi, K. Adachi, I. Yamada, K. N. Sato, K. Kawahata, A. Nishizawa, S. Ohdachi, K. Sato, T. Seki, T. Watari, J. Xu, A. Ejiri, S. Hirokura, K. Ida, Y. Kawasumi, M. Kojima, H. Sakakita, T. Ido, K. Kitachi, J. Koog and H. Kuramoto,
Observation of Dusts by Laser Scattering Method in theJIPPT-IIU Tokamak Mar. 1997

NIFS-486 S. Bazdenkov, T. Sato and The Complexity Simulation Group,
Topological Transformations in Isolated Straight Magnetic Flux Tube; Mar. 1997

NIFS-487 M. Okamoto,
Configuration Studies of LHD Plasmas; Mar. 1997

NIFS-488 A. Fujisawa, H. Iguchi, H. Sanuki, K. Itoh, S. Lee, Y. Hamada, S. Kubo, H. Idei, R. Akiyama, K. Tanaka, T. Minami, K. Ida, S. Nishimura, S. Morita, M. Kojima, S. Hidekuma, S.-I. Itoh, C. Takahashi, N. Inoue, H. Suzuki, S. Okamura and K. Matsuoka,
Dynamic Behavior of Potential in the Plasma Core of the CHS Heliotron/Torsatron; Apr. 1997

NIFS-489 T. Ohkawa,
Pfirsch - Schlüter Diffusion with Anisotropic and Nonuniform Superthermal Ion Pressure; Apr. 1997

NIFS-490 S. Ishiguro and The Complexity Simulation Group,
Formation of Wave-front Pattern Accompanied by Current-driven Electrostatic Ion-cyclotron Instabilities; Apr. 1997

NIFS-491 A. Ejiri, K. Shinohara and K. Kawahata,
An Algorithm to Remove Fringe Jumps and its Application to Microwave Reflectometry; Apr. 1997

NIFS-492 K. Ichiguchi, N. Nakajima, M. Okamoto,
Bootstrap Current in the Large Helical Device with Unbalanced Helical Coil Currents; Apr. 1997

NIFS-493 S. Ishiguro, T. Sato, H. Takamaru and The Complexity Simulation Group,
V-shaped dc Potential Structure Caused by Current-driven Electrostatic Ion-cyclotron Instability; May 1997

NIFS-494 K. Nishimura, R. Horiuchi, T. Sato,
Tilt Stabilization by Energetic Ions Crossing Magnetic Separatrix in Field-Reversed Configuration; June 1997

NIFS-495 T. -H. Watanabe and T. Sato,
Magnetohydrodynamic Approach to the Feedback Instability; July 1997

NIFS-496 K. Itoh, T. Ohkawa, S. -I.Itoh, M. Yagi and A. Fukuyama
Suppression of Plasma Turbulence by Asymmetric Superthermal Ions; July 1997

NIFS-497 T. Takahashi, Y. Tomita, H. Momota and Nikita V. Shabrov,
Collisionless Pitch Angle Scattering of Plasma Ions at the Edge Region of an FRC; July 1997

NIFS-498 M. Tanaka, A.Yu Grosberg, V.S. Pande and T. Tanaka,
Molecular Dynamics and Structure Organization in Strongly-Coupled Chain of Charged Particles; July 1997